nature geoscience

Article

https://doi.org/10.1038/s41561-023-01355-4

Formation of secondary organic aerosol from wildfire emissions enhanced by long-time ageing

Received: 31 August 2023

Accepted: 7 December 2023

Published online: 9 January 2024

Check for updates

Yicong He[1,2], Bin Zhao[1,2] ✉, Shuxiao Wang[1,2], Richard Valorso[3], Xing Chang[1,2], Dejia Yin[1,2], Boyang Feng[1,2], Marie Camredon[3], Bernard Aumont[3], Abraham Dearden[4], Shantanu H. Jathar[4], Manish Shrivastava[5], Zhe Jiang[6], Christopher D. Cappa[7], Lindsay D. Yee[8], John H. Seinfeld[9], Jiming Hao[1,2] & Neil M. Donahue[10]

Wildfire smoke, consisting primarily of organic aerosols, has profound impacts on air quality, climate and human health. Wildfire organic aerosol evolves over long-time photochemical oxidation due to the formation and ageing of secondary organic aerosol, which substantially changes its magnitude and properties. However, there are large uncertainties in the long-time ageing of wildfire organic aerosol because of the distinct ageing behaviours of the complex organic emissions. Here we developed an oxidation model that simulates the ageing of wildfire organic emissions in the full volatility range on a precursor level and integrated insights from single-species ageing and wildfire emissions ageing experiments and field plume observations to constrain the long-time ageing of wildfire organic aerosol. The model captured the enhancement of organic aerosol mass (2–8 times) and oxygen-to-carbon ratio (1–4 times) in the wildfire ageing experiments. It also reconciled a long-standing discrepancy between field and laboratory observations of the magnitude of secondary organic aerosol formation. The model indicated large emissions-driven variations in precursor contributions to secondary organic aerosol, which further evolve with long-time ageing. The estimated global wildfire secondary organic aerosol production (139 ± 34 Tg per year) was much higher than previous studies omitting or under-constraining long-time ageing.

Wildfires burn through 3.5% of the Earth's ice-free land surface each year on average[1], emitting large amounts of primary aerosols and precursors that can be oxidized to form secondary aerosols, resulting in important environmental consequences[2]. For example, wildfire smoke causes about 340,000 premature deaths each year globally through affecting human respiratory and cardiovascular systems[3]. It also interacts with solar radiation and affects cloud formation, resulting in a radiative forcing of up to −0.5 W m^{-2}, offsetting 25% of the forcing by CO_2 (~2 W m^{-2}) (ref. 4). The influence of wildfires is expected to increase in the future with a warming climate[5].

[1]State Key Joint Laboratory of Environmental Simulation and Pollution Control, School of Environment, Tsinghua University, Beijing, China. [2]State Environmental Protection Key Laboratory of Sources and Control of Air Pollution Complex, Beijing, China. [3]Université Paris-Est Créteil and Université Paris Cité, CNRS, LISA, Créteil, France. [4]Department of Mechanical Engineering, Colorado State University, Fort Collins, CO, USA. [5]Pacific Northwest National Laboratory, Richland, WA, USA. [6]Carbon Neutrality Research Center, Institute of Atmospheric Physics, Chinese Academy of Sciences, Beijing, China. [7]Civil and Environmental Engineering, University of California Davis, Davis, CA, USA. [8]Department of Environmental Science, Policy and Management, University of California Berkeley, Berkeley, CA, USA. [9]Department of Chemical Engineering, California Institute of Technology, Pasadena, CA, USA. [10]Center for Atmospheric Particle Studies, Carnegie Mellon University, Pittsburgh, PA, USA. ✉e-mail: bzhao@mail.tsinghua.edu.cn

https://doi.org/10.1038/s41561-023-01355-4

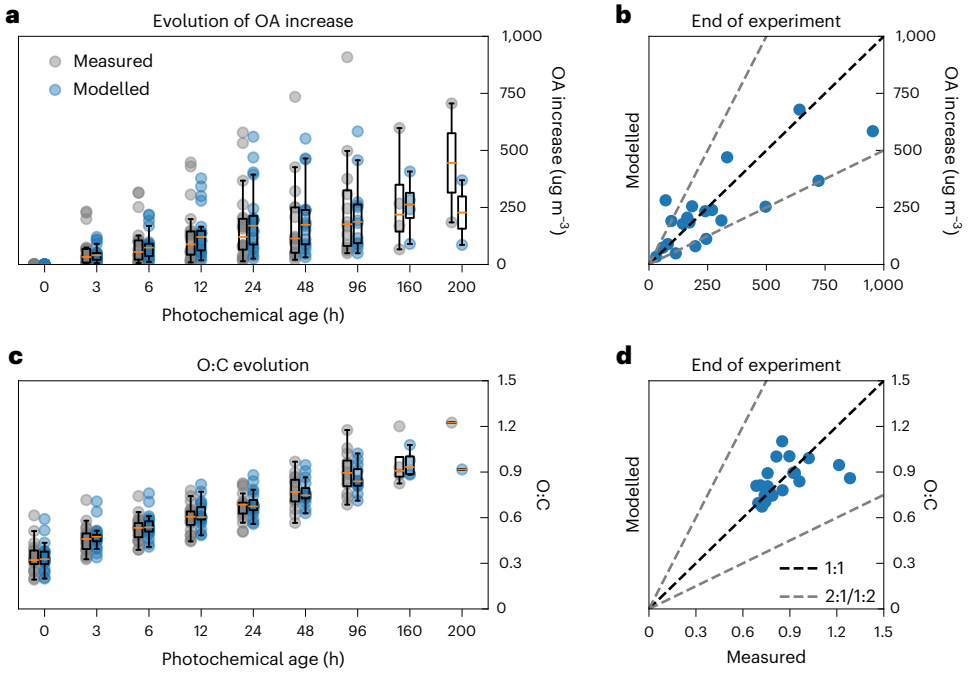

Fig. 1 | Modelling the FIREX mini-chamber experiments[17]. Model–measurement comparisons are shown for changes in OA mass concentrations (with respect to the initial values) and O:C, respectively. **a**,**c**, The comparison at different photochemical ages. **b**,**d**, The comparison at the end of the experiments. The box plots in **a** and **c** show distributions of each group of data points, including 20 experiments, at the 5% (lower whisker), 25% (box lower bound), 50% (box centre line), 75% (box upper bound) and 95% (upper whisker) percentiles. The photochemical age is the integrated OH exposure divided by a typical atmospheric OH level (1.5×10^6 molecules cm^{-3}).

Wildfire smoke is dominated by organic aerosol (OA) (70–80% by mass)[6–9] with atmospheric lifetimes of over one week[2]. During this time, the emitted gas-phase organic compounds and those evaporated from primary OA (POA) can be photochemically aged to form secondary OA (SOA), with up to 90% of the SOA originating from the ageing of intermediate and semi-volatile organic compounds (I/SVOC; saturation vapour concentration C^* between 10^4 and 10^6 μg m^{-3}) (ref. 10). Because the magnitude and properties (for example, light absorptivity and hygroscopicity) of SOA substantially evolve with ageing[11–19], long-time ageing largely determines the air quality and climate impacts of wildfires, as opposed to the first few hours of ageing, which have been the focus of most previous studies[20]. Despite the importance of long-time ageing of wildfire OA, it still has many uncertainties, as demonstrated by an unresolved laboratory–field gap in the net increase of wildfire OA with ageing (minimal in field and higher in laboratory studies)[1,2]; and by wide-ranging estimates of global wildfire SOA production[2].

Earlier studies (for example, refs. 21,22) mostly did not account for the long-time ageing of wildfire OA. Some later studies (for example, refs. 4,23) accounted for this process but simplistically modelled chemically complex I/SVOCs as a single type of species and did not constrain the ageing behaviours against experiments. For example, Hodzic et al.[23] simulated the ageing of I/SVOCs using alkanes as a proxy, which typically have lower SOA-forming potentials than wildfire I/SVOC compositions (for example, phenols). Shrivastava et al.[4] modelled the ageing of all I/SVOCs with a single set of empirical parameters that were not informed by experiments. These studies gave a wide uncertain range of estimated global wildfire SOA production (15–250 Tg per year). In reality, I/SVOCs are composed of hundreds of species that vary substantially with fuel types and burning conditions[24], and different species have distinct ageing behaviours with SOA formation potentials spanning over an order of magnitude[19,25]. Thus, there is a need to accurately predict the evolution of wildfire OA by constraining the long-time ageing of SOA precursors on the level of individual species or at least species types. A couple of studies[18,19,26] investigated the wildfire SOA formation from different types of species but were limited to short ageing times.

Here we developed an oxidation model, namely precursor-resolved 2D-VBS-MOSAIC (Two-dimensional Volatility Basis Set and Model for Simulating Aerosol Interaction and Chemistry), to separately simulate the ageing of different precursors including I/SVOCs. Long-time evolution of wildfire SOA was investigated with the model with integrated insights from long-time single-precursor and wildfire emissions ageing experiments and field observations of wildfire plumes. The model consistently captured wildfire SOA formation in long-time ageing experiments and real plumes and reconciled the long-standing discrepancy in SOA formation between laboratory and field studies by elucidating the important roles of plume dilution, emissions variability and how close flights can sample fire emissions. The model revealed that there are substantial changes in precursor contributions to SOA with long-time ageing and estimated that the global wildfire SOA production was much higher than previous estimates under-constraining ageing over atmospherically relevant timescales.

Capturing long-time laboratory ageing of wildfire OA

We updated the 2D-VBS model to simulate the multi-generational ageing of individual SOA precursors, including I/SVOCs, by constraining their first-generation oxidation through explicit chemical mechanisms informed by GECKO-A (the Generator for Explicit Chemistry and Kinetics of Organics in the Atmosphere)[27] and later-generation oxidation through optimized ageing parameterizations specific to each precursor chemical class. These precursor classes included oxygenated aromatics (for example, phenols), heterocyclics (for example, furans), polycyclic aromatics, benzene-series aromatics, alkanes, terpenes and other semi- and low-volatile organic compounds (S/L-VOC) evaporated from POA. More details on the model and the optimization of the ageing parameters can be found in Methods. The model was applied to simulate a suite of 20 wildfire emissions ageing

https://doi.org/10.1038/s41561-023-01355-4

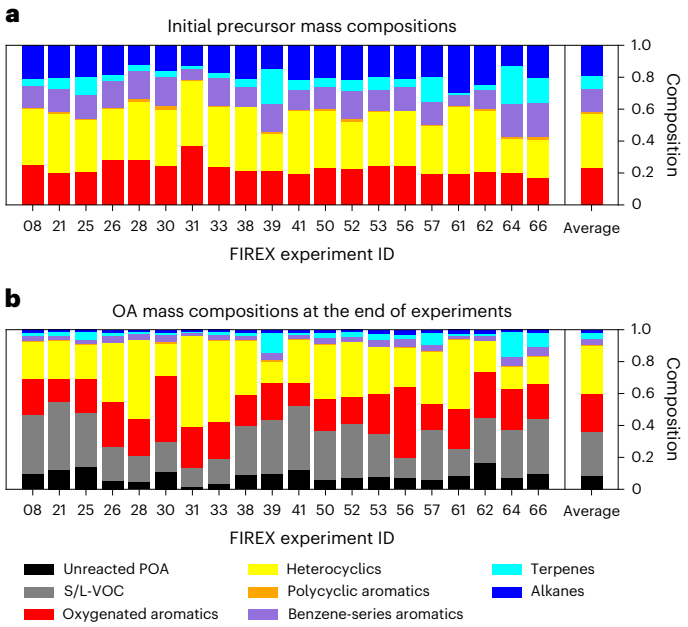

Fig. 2 | Precursor composition and contributions to SOA. a,**b**, Initial precursor composition (**a**) and predicted final OA mass composition (**b**) for the 20 FIREX mini-chamber experiments. The average across all experiments is shown by the standalone columns on the right.

experiments from the FIREX (Fire Influence on Regional and Global Environments) 2016 campaign inside the 'mini chamber', which covered various biomass fuels (for example, pines, grasses, shrubs and so on) and burning conditions (smouldering to flaming)[17]. Wildfire emissions, including gas-phase compositions and POA concentrations, were characterized in these experiments before being aged for an equivalent photochemical age of up to 200 hours (assuming atmospheric OH = 1.5×10^6 molecules cm^{-3}) to quantify the amount of SOA formation (corrected for chamber dilution and particle wall loss (PWL)) and its O:C ratio. The measured emissions profiles (Supplementary Table 3) were used as model input and the predicted OA was corrected for PWL and dilution for comparison with observations. More details of the mini-chamber experiments and the model configurations can be found in Methods.

Figure 1 shows the model–measurement comparisons for the OA mass enhancement with respect to time zero and for O:C. Figure 1a,c suggests that the model was able to follow the increasing trend of both OA mass enhancement and O:C on average over long-time ageing with no large bias (normalized mean bias over all photochemical ages is −7% for OA mass enhancement and −2% for O:C). The comparison at the end of experiments, in Fig. 1b,d, showed moderate scatter for OA mass enhancement and O:C, but they are generally bounded within a factor of two. The less scatter for O:C suggests the model captures well the ageing processes, and the scatter in OA mass enhancement agreement may be related to the uniform assumption of PWL rate applied to these experiments when correcting the raw OA measurements for PWL, whereas experiment-specific PWL rates could vary substantially due to particle charges and chamber turbulent level[17,28,29]. Overall, there is substantial SOA formation from wildfire emission ageing, and the model can capture the long-time ageing behaviour of the complex mixture of wildfire emissions.

Figure 2 shows the gaseous precursor compositions at the beginning of the experiments and their predicted final contributions to OA mass for the 20 FIREX mini-chamber experiments. The initial gaseous precursors contained large fractions of heterocyclic (34.0 ± 5.9%) and oxygenated aromatic species (23.1 ± 4.4%), with important contributions from benzene-series aromatics (14.9 ± 3.7%), alkanes (19.3 ± 4.1%) and terpenes (7.8 ± 6.5%). The plus–minus sign shows one standard deviation across all experiments here and after. After ageing, only oxygenated aromatics (32.7 ± 12.2%) and heterocyclics (26.3 ± 8.4%) contributed greatly to SOA due to the distinct ageing rates and SOA-forming potentials of different SOA precursors (Supplementary Figs. 1 and 2)[16,18,19,26], which suggests that assuming wildfire I/SVOCs to be alkanes, as in previous studies[23], will lead to low biases in SOA production. Moreover, evaporated POA (S/L-VOCs) also contributed greatly to SOA (30.2 ± 10.7%) due to ageing in the gas phase. Unreacted POA, however, accounted for only a small fraction of total OA by the end of the experiments, consistent with previous laboratory experiments that estimated POA using levoglucosan as a tracer[14]. In addition, across individual experiments, there were large variations in precursor contributions, with heterocyclics, for example, accounting for between 10% and 50% of SOA. The difference can be attributed to the different initial precursor compositions, which were driven by various fuel types and burning conditions (Supplementary Table 2). Overall, precursor-level resolution is necessary to reflect the dynamics of wildfire SOA composition and associated properties.

Reconciling laboratory and field wildfire OA formation

Understanding the atmospheric evolution of wildfire OA based on laboratory studies requires consistent oxidation chemistry between the two conditions. However, current laboratory and field observations show systematic differences in SOA formation, as measured by ΔOA/ΔCO (the CO-normalized excess mixing ratio of OA, where excess mixing ratio means the difference between in-plume and background mixing ratios): field studies report ΔOA/ΔCO enhancement of around 1 on average, but laboratory studies report 1.26[1], which could be even higher by up to two times if accounting for wall loss effects[30]. Some studies investigated dilution-driven POA evaporation in field to explain this gap[31–33], but there remain other untested main hypotheses, including emissions variabilities and missed initial SOA formation and precursor depletion due to distance between fire origin and first flight transects of plumes. To note, initial OA reference distanced from the fire origin causes lower apparent SOA formation. Here we systematically assess these main hypotheses[1] and try to close the field–laboratory gap.

We simulated airborne observations of wildfire plumes summarized by Hodshire et al.[1], where specific OH levels and dilution rates were applied to each plume. Because there lacked comprehensive emissions profiles for the real plumes, we simulated each plume with the 20 FIREX emissions profiles to capture potential variability in precursor composition. In Fig. 3a, we compare observed ΔOA/ΔCO enhancement ratios at the farthest flight transect with model predictions under different scenarios, including dilution only, ageing only and stepwise inclusion of adjusted initial reference point (that is, $t_{1st,phys}$ reported in Supplementary Table 4), dilution and emissions variability on top of the ageing-only scenario. Average ΔOA/ΔCO value across the 20 repetitions is shown (Methods). For most of the plumes, the ageing-only and dilution-only scenarios bounded the observations, and the combination of right initial timing and dilution substantially reduced the gap with observations for most campaigns. The influences of these two corrections varied between campaigns, with some showing dominant influence from initial timing (for example, Garofalo et al.[34] and Liu et al.[35]) and some from dilution (for example, Akagi et al.[36]), or roughly equal from both (for example, Yokelson et al.[11]). Finally, the variability due to emissions profiles seemed to vary across campaigns, and in some cases, its influence was as large as those of dilution and timing of initial measurement, whereas in others, its influence was smaller. Overall, the model was able to reconcile laboratory-based predictions (that is, the 'ageing-only' case) with field observations of wildfire SOA formation, as shown in Fig. 3b. It showed that plume dilution, offset in initial flight measurements and emissions variability can all contribute to the laboratory–field

https://doi.org/10.1038/s41561-023-01355-4

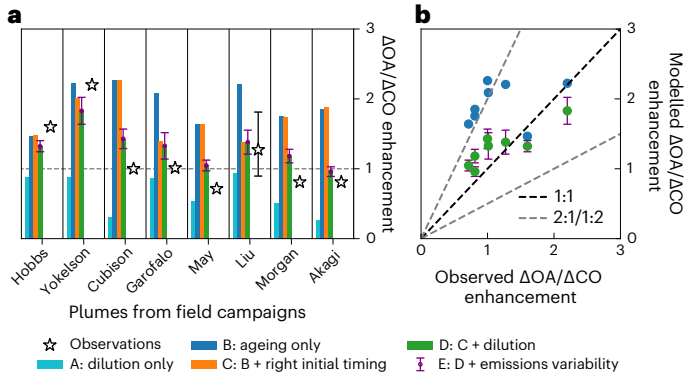

Fig. 3 | Modelling SOA formation in wildfire plumes. a, Model prediction of OA enhancement in wildfire plumes at the farthest flight transects, represented by the normalized excess mixing ratio with respect to CO (ΔOA/ΔCO). Each observation was simulated with plume-specific OH level and dilution rates. For each plume, two bounding cases are shown ('dilution only' and 'ageing only'), and the influences of dilution, timing of initial measurement and emissions variability are accounted for cumulatively on the 'ageing-only' case. For the 'dilution-only' and 'ageing-only' cases, the initial ΔOA/ΔCO was taken at $t = 0$. **b**, The model–measurement comparison for the 'ageing-only' case and the 'all-included' case to visualize improvement in predictions. The predictions from the 'emissions variability' cases are shown as mean values ± one standard deviation, including predictions from 20 emissions profiles. The observations from Liu et al. included five plumes and are shown as the 5% percentile, the mean and the 95% percentile. The references include the following: refs. 11,34–36,39,46–49.

gap, with varying importance depending on specific plumes, unlike previous studies stressing dilution only[32].

Atmospheric wildfire SOA evolution and global production

We estimated the average wildfire SOA evolution in the atmosphere over 200 equivalent hours of ageing (assuming atmospheric OH level of 1.5×10^6 molecules cm^{-3}) by performing Monte Carlo simulations that accounted for variations in emissions profiles, dilution rates and OH levels. We assumed that the FIREX-average emissions profile, with scaled-up one standard deviation, encompassed the global-average profile and its variability, which was validated by comparison with an estimated global-average profile for shared species. More details of the Monte Carlo simulations, the global-average profile and the estimation of the variability in dilution rates and OH concentrations can be found in Methods. We performed a sensitivity simulation where we applied biome-specific emissions ratios of available SOA precursors to the FIREX-average emission profile (Methods) and the model predictions of SOA only varied moderately (Supplementary Fig. 3).

Figure 4a shows the average evolution of the ΔOA/ΔCO enhancement ratio, resolved by contributions from precursor classes (normalized in bottom panel). The level of enhancement increased throughout most of the ageing time, reaching a maximum of 4.4 at around 100 hours of ageing and stayed relatively constant after that. Simultaneously, the O:C ratio substantially increased from 0.5 to 1, implying highly hygroscopic aged wildfire OA[37]. Note that the predicted ΔOA/ΔCO at higher ageing times, as shown in Extended Data Fig. 1, is in close agreement with measurements inside the highly aged biomass-burning OA layer in the free troposphere above western Africa[38]. As for compositions, POA initially accounted for >95% of OA mass, but SOA quickly accounted for 40–50% of OA mass by two hours of ageing due to POA evaporation and SOA production, including that from evaporated POA species (that is, S/L-VOCs). At the end, SOA accounted for nearly 90% of OA mass. The results here support that wildfire OA is dominated by SOA at longer photochemical ages, with substantial changes in OA oxidation state driven by photochemical ageing[1].

The dominant contributors to SOA at the end were S/L-VOCs (40.1 ± 10.2%), heterocyclics (27.6 ± 6.7%) and oxygenated aromatics (18.5 ± 5.5%). The contributions clearly depended on photochemical age. The S/L-VOC contribution increased continuously, which is driven by the sustained dilution of the plume, causing a large fraction of POA to evaporate and become oxidized. At lower ageing times (<1 day),

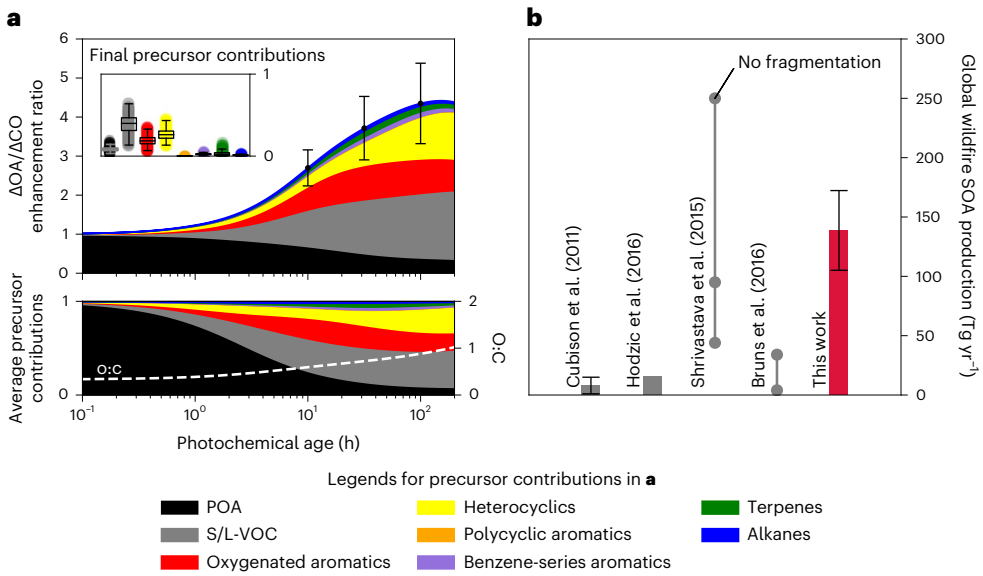

Fig. 4 | Modelling global SOA production. a, Monte Carlo simulation of average ΔOA/ΔCO enhancement and O:C from wildfire plumes in the atmosphere through randomly sampled emissions profiles, dilutions rates and OH levels; the bottom panel shows average precursor contributions to OA with ageing time; the inset shows the scatter in precursor contributions at the end of ageing. **b**, Estimated global SOA production from wildfires in comparison to previous studies. In **a** and **b**, the predicted ΔOA/ΔCO enhancement ratio and SOA production are shown as mean values ± one standard deviation, including predictions from 500 Monte Carlo simulations. For Cubison et al.[39], the estimated production is shown as mean value ± one standard deviation, and for details, see the reference. In the inset of **a**, the box plots show 500 simulated contribution fractions for each precursor class at the 5% (lower whisker), 25% (box lower bound), 50% (box centre line), 75% (box upper bound) and 95% (upper whisker) percentiles. For Shrivastava et al.[4], the lower two points represent the maximal range of prediction, whereas the top point represents an upper-limit case with no fragmentation. For Bruns et al.[16], the two points represent the maximal range. The references include: refs. 4,16,23,39.

oxygenated aromatics were more important than heterocyclics (200% of heterocyclics), but at higher ageing times (up to 200 hours), heterocyclics contributed more SOA (138% of oxygenated aromatics). This is explained by the lower chance of fragmentation (that is, higher m_{FRAG} value) for the heterocyclic class (Supplementary Table 1). The contribution from the other classes remained low. The results suggest that precursor contributions vary substantially with long-time ageing.

Figure 4b shows our estimated global production of wildfire SOA based on a POA source strength of 23–41 Tg per year, which is the typical range in previous studies[4,16,23,39], and the maximal OA enhancement ratio predicted above. The estimates are compared with those from previous works[4,16,23,39]. Our mean estimate was 139 ± 34 Tg per year, which was at the higher end of the compiled data. Of the previous studies, Cubison et al.[39] and Bruns et al.[16] discounted long-time ageing, which explains the lower estimates. Hodzic et al.[23] and Shrivastava et al.[4] simulated long-time ageing with lumped I/SVOCs by either regarding all I/SVOCs as linear alkanes (typically low in SOA-forming potentials) or used under-constrained ageing parameters, and this contributes to the wide-ranging wildfire SOA production estimates (15–250 Tg per year; note the upper bound of 250 Tg per year tested the sensitivity of no-fragmentation reactions). Overall, the results here suggest that wildfire SOA may be much more important (1.5–17 times) than previously estimated (discounting the no-fragmentation case). Note that our SOA production would decrease by 23% if POA is not allowed to evaporate and form S/L-VOC SOA, as was the case for the some previous studies[4,23], but this would not change our overall higher predictions than the previous ones.

Atmospheric implications of long-time ageing of wildfire OA

The newly developed precursor-resolved 2D-VBS-MOSAIC model achieved good closure with wildfire long-time ageing experiments, revealed large variations in precursor contributions with ageing, reconciled the laboratory–field difference in SOA formation and reduced uncertainties in atmospheric SOA evolution. In contrast, by lumping I/SVOCs (for example, as pentadecane) as in traditional studies, the model showed much worse performance in capturing SOA mass and O:C (Extended Data Fig. 2), compared with Fig. 1.

We showed that wildfire SOA evolves substantially with long-time ageing in terms of magnitude, oxidation state and precursor contributions, with great implications for air quality, climate and human health. For example, strong SOA formation makes wildfires possibly the most important source of global SOA production. On the basis of 'top-down' ambient- and remote-sensing data[23], our estimated wildfire SOA production (139 ± 34 Tg per year) explains at least 30% of global SOA production. This suggests that wildfire OA may be much more abundant in the atmosphere than estimated before[4,16,23,39]. In addition, continued SOA production sustains elevated levels of wildfire smoke, allowing it to be transported farther and to have more regionally spread-out air quality and climate effects. The increase in oxidation state suggests that wildfire OA becomes highly hygroscopic (O:C ~ 1), making them more prone to activate as cloud condensation nuclei. The changes in precursor contributions may impact the optical and toxicological properties of wildfire OA; specifically, light-absorbing brown carbon has been largely associated with secondary nitro products from oxygenated aromatics[40], and the health-relevant aerosol oxidative potential has been associated with aromatic products in general[41]. Overall, our results help better quantify the health and climate impacts of wildfires and suggest that these impacts may be underestimated in most previous studies. Future works on the impacts of wildfire SOA would require integration of our model into a three-dimensional model after proper simplification; this is feasible based on our previous studies[42,43] that performed three-dimensional simulations with the 2D-VBS framework.

Fossil fuel combustion and volatile chemical products are also SOA sources with large amounts of I/SVOCs[44,45]. Extended Data Fig. 3 demonstrates that SOA from these sectors vary greatly in yield and precursor contributions; for example, the difference in SOA yield can be as large as three times between different sectors. This may significantly change SOA source attributions based on uniform treatment of I/SVOCs without considering the variation in precursor contributions. Our improved ageing scheme may enable atmospheric models to better resolve the sector and precursor contributions to ambient SOA, which serves as the basis for mitigation policymaking.

Online content

Any methods, additional references, Nature Portfolio reporting summaries, source data, extended data, supplementary information, acknowledgements, peer review information; details of author contributions and competing interests; and statements of data and code availability are available at https://doi.org/10.1038/s41561-023-01355-4.

References

1. Hodshire, A. L. et al. Aging effects on biomass burning aerosol mass and composition: a critical review of field and laboratory studies. *Environ. Sci. Technol.* **53**, 10007–10022 (2019).
2. Shrivastava, M. et al. Recent advances in understanding secondary organic aerosol: implications for global climate forcing. *Rev. Geophys.* **55**, 509–559 (2017).
3. Johnston, F. H. et al. Estimated global mortality attributable to smoke from landscape fires. *Environ. Health Perspect.* **120**, 695–701 (2012).
4. Shrivastava, M. et al. Global transformation and fate of SOA: implications of low-volatility SOA and gas-phase fragmentation reactions: global Modeling of SOA. *J. Geophys. Res. Atmos.* **120**, 4169–4195 (2015).
5. Westerling, A. L. Increasing western US forest wildfire activity: sensitivity to changes in the timing of spring. *Phil. Trans. R. Soc. B* **371**, 20150178 (2016).
6. Andreae, M. O. & Merlet, P. Emission of trace gases and aerosols from biomass burning. *Glob. Biogeochem. Cycles* **15**, 955–966 (2001).
7. Van Der Werf, G. R. et al. Global fire emissions and the contribution of deforestation, savanna, forest, agricultural, and peat fires (1997–2009). *Atmos. Chem. Phys.* **10**, 11707–11735 (2010).
8. Wiedinmyer, C. et al. The Fire INventory from NCAR (FINN): a high resolution global model to estimate the emissions from open burning. *Geosci. Model Dev.* **4**, 625–641 (2011).
9. Andreae, M. O. et al. Aerosol characteristics and particle production in the upper troposphere over the Amazon Basin. *Atmos. Chem. Phys.* **18**, 921–961 (2018).
10. Robinson, A. L. et al. Rethinking organic aerosols: semivolatile emissions and photochemical aging. *Science* **315**, 1259–1262 (2007).
11. Yokelson, R. J. et al. Emissions from biomass burning in the Yucatan. *Atmos. Chem. Phys.* **9**, 5785–5812 (2009).
12. Vakkari, V. et al. Rapid changes in biomass burning aerosols by atmospheric oxidation. *Geophys. Res. Lett.* **41**, 2644–2651 (2014).
13. Vakkari, V. et al. Major secondary aerosol formation in southern African open biomass burning plumes. *Nat. Geosci.* **11**, 580–583 (2018).
14. Hennigan, C. J. et al. Chemical and physical transformations of organic aerosol from the photo-oxidation of open biomass burning emissions in an environmental chamber. *Atmos. Chem. Phys.* **11**, 7669–7686 (2011).
15. Ortega, A. M. et al. Secondary organic aerosol formation and primary organic aerosol oxidation from biomass-burning smoke in a flow reactor during FLAME-3. *Atmos. Chem. Phys.* **13**, 11551–11571 (2013).
16. Bruns, E. A. et al. Identification of significant precursor gases of secondary organic aerosols from residential wood combustion. *Sci. Rep.* **6**, 27881 (2016).

17. Lim, C. Y. et al. Secondary organic aerosol formation from the laboratory oxidation of biomass burning emissions. *Atmos. Chem. Phys.* **19**, 12797–12809 (2019).
18. Ahern, A. T. et al. Production of secondary organic aerosol during aging of biomass burning smoke from fresh fuels and its relationship to VOC precursors. *J. Geophys. Res. Atmos.* **124**, 3583–3606 (2019).
19. Akherati, A. et al. Oxygenated aromatic compounds are important precursors of secondary organic aerosol in biomass-burning emissions. *Environ. Sci. Technol.* **54**, 8568–8579 (2020).
20. Tsigaridis, K. et al. The AeroCom evaluation and intercomparison of organic aerosol in global models. *Atmos. Chem. Phys.* **14**, 10845–10895 (2014).
21. Spracklen, D. V. et al. Aerosol mass spectrometer constraint on the global secondary organic aerosol budget. *Atmos. Chem. Phys.* **11**, 12109–12136 (2011).
22. Pye, H. O. T. & Seinfeld, J. H. A global perspective on aerosol from low-volatility organic compounds. *Atmos. Chem. Phys.* **10**, 4377–4401 (2010).
23. Hodzic, A. et al. Rethinking the global secondary organic aerosol (SOA) budget: stronger production, faster removal, shorter lifetime. *Atmos. Chem. Phys.* **16**, 7917–7941 (2016).
24. Andreae, M. O. Emission of trace gases and aerosols from biomass burning—an updated assessment. *Atmos. Chem. Phys.* **19**, 8523–8546 (2019).
25. Yee, L. D. et al. Secondary organic aerosol formation from biomass burning intermediates: phenol and methoxyphenols. *Atmos. Chem. Phys.* **13**, 8019–8043 (2013).
26. Stefenelli, G. et al. Secondary organic aerosol formation from smoldering and flaming combustion of biomass: a box model parametrization based on volatility basis set. *Atmos. Chem. Phys.* **19**, 11461–11484 (2019).
27. Aumont, B., Szopa, S. & Madronich, S. Modelling the evolution of organic carbon during its gas-phase tropospheric oxidation: development of an explicit model based on a self generating approach. *Atmos. Chem. Phys.* **5**, 2497–2517 (2005).
28. Bian, Q., May, A. A., Kreidenweis, S. M. & Pierce, J. R. Investigation of particle and vapor wall-loss effects on controlled wood-smoke smog-chamber experiments. *Atmos. Chem. Phys.* **15**, 11027–11045 (2015).
29. He, Y. et al. Secondary organic aerosol formation from evaporated biofuels: comparison to gasoline and correction for vapor wall losses. *Environ. Sci. Processes Impacts* **22**, 1461–1474 (2020).
30. Bilsback, K. R. et al. Vapors are lost to walls, not to particles on the wall: artifact-corrected parameters from chamber experiments and implications for global secondary organic aerosol. *Environ. Sci. Technol.* https://doi.org/10.1021/acs.est.2c03967 (2022).
31. Bian, Q. et al. Secondary organic aerosol formation in biomass-burning plumes: theoretical analysis of lab studies and ambient plumes. *Atmos. Chem. Phys.* **17**, 5459–5475 (2017).
32. Hodshire, A. L. et al. More than emissions and chemistry: fire size, dilution, and background aerosol also greatly influence near-field biomass burning aerosol aging. *J. Geophys. Res. Atmos.* **124**, 5589–5611 (2019).
33. Akherati, A. et al. Dilution and photooxidation driven processes explain the evolution of organic aerosol in wildfire plumes. *Environ. Sci. Atmos.* https://doi.org/10.1039/D1EA00082A (2022).
34. Garofalo, L. A. et al. Emission and evolution of submicron organic aerosol in smoke from wildfires in the western United States. *ACS Earth Space Chem.* **3**, 1237–1247 (2019).
35. Liu, X. et al. Agricultural fires in the southeastern U.S. during SEAC ^{4} RS: emissions of trace gases and particles and evolution of ozone, reactive nitrogen, and organic aerosol. *J. Geophys. Res. Atmos.* **121**, 7383–7414 (2016).
36. Akagi, S. K. et al. Evolution of trace gases and particles emitted by a chaparral fire in California. *Atmos. Chem. Phys.* **12**, 1397–1421 (2012).
37. Lambe, A. T. et al. Laboratory studies of the chemical composition and cloud condensation nuclei (CCN) activity of secondary organic aerosol (SOA) and oxidized primary organic aerosol (OPOA). *Atmos. Chem. Phys.* **11**, 8913–8928 (2011).
38. Haslett, S. L. et al. Remote biomass burning dominates southern West African air pollution during the monsoon. *Atmos. Chem. Phys.* **19**, 15217–15234 (2019).
39. Cubison, M. J. et al. Effects of aging on organic aerosol from open biomass burning smoke in aircraft and laboratory studies. *Atmos. Chem. Phys.* **11**, 12049–12064 (2011).
40. Laskin, A., Laskin, J. & Nizkorodov, S. A. Chemistry of atmospheric brown carbon. *Chem. Rev.* **115**, 4335–4382 (2015).
41. Tuet, W. Y. et al. Chemical oxidative potential of secondary organic aerosol (SOA) generated from the photooxidation of biogenic and anthropogenic volatile organic compounds. *Atmos. Chem. Phys.* **17**, 839–853 (2017).
42. Zhao, B. et al. High concentration of ultrafine particles in the Amazon free troposphere produced by organic new particle formation. *Proc. Natl Acad. Sci. USA* **117**, 25344–25351 (2020).
43. Chang, X. et al. Full-volatility emission framework corrects missing and underestimated secondary organic aerosol sources. *One Earth* **5**, 403–412 (2022).
44. Drozd, G. T. et al. Detailed speciation of intermediate volatility and semivolatile organic compound emissions from gasoline vehicles: effects of cold-starts and implications for secondary organic aerosol eormation. *Environ. Sci. Technol.* **53**, 1706–1714 (2019).
45. McDonald, B. C. et al. Volatile chemical products emerging as larges petrochemical source of urban organic emissions. *Science* **359**, 760–764 (2018).
46. Hobbs, P. V. et al. Evolution of gases and particles from a savanna fire in South Africa. *J. Geophys. Res.* **108**, 8485 (2003).
47. May, A. A. et al. Observations and analysis of organic aerosol evolution in some prescribed fire smoke plumes. *Atmos. Chem. Phys.* **15**, 6323–6335 (2015).
48. Morgan, W. T. et al. Transformation and ageing of biomass burning carbonaceous aerosol over tropical South America from aircraft in situ measurements during SAMBBA. *Atmos. Chem. Phys.* **20**, 5309–5326 (2020).
49. Alvarado, M. J. & Prinn, R. G. Formation of ozone and growth of aerosols in young smoke plumes from biomass burning: 1. Lagrangian parcel studies. *J. Geophys. Res.* **114**, D09306 (2009).

Methods

Precursor-resolved 2D-VBS-MOSAIC model

In this work, we coupled the 2D-VBS[50–52] (Two-dimensional Volatility Basis Set) model with the MOSAIC[53] model (Model for Simulating Aerosol Interactions and Chemistry) to form the basis of our new model development. The 2D-VBS model simulates gas-phase multi-generational ageing driven by OH, and the MOSAIC model focuses on gas/particle partitioning and other particle-phase kinetic processes. The 2D-VBS model does not account for inorganic photochemistry and uses externally prescribed OH concentrations. We made further model developments to allow for explicit consideration of first-generation oxidation products from individual precursors and precursor-class-specific ageing of later-generation organic compounds. MOSAIC was updated to simulate kinetic heterogeneous oxidation. These aspects of the model are discussed in detail below.

The 2D-VBS distils the complex mixture of organic compounds from multi-generational photochemical ageing into two dimensions, volatility (that is, C^*) and oxidation state (that is, O:C). A two-dimensional space defined by C^* (herein covering −10 to 8 in $\log_{10}$ of μg m^{-3}) and O:C (herein covering 0 to 2) is discretized into evenly spaced 'cells' (increment of 1 in $\log_{10}$ of C^* and 0.1 in O:C), also called 2D-VBS 'products', so that the matrix of products represents all possible organic compounds and each product represents a statistical average over the compounds in its vicinity. The model accounts for functionalization and fragmentation reactions of each product, leading to the formation of other 2D-VBS products. The reaction probabilities and product distributions are controlled by model parameterizations. For fragmentation, x_{FRAG} controls the probability through $p_{FRAG} = (O{:}C \times 0.5)^{xFRAG}$. The fragmentation product distribution is the same as in Chuang and Donahue[50]. For functionalization, the probability is the complement of fragmentation ($p_{FUNC} = 1 - p_{FRAG}$) and the product distribution has been modified to include more adjustable parameters; the probabilities of the species adding 1, 2, 3 or 4 oxygens are p_{O1}, p_{O2}, p_{O3} and p_{O4}, respectively, and the decrease in volatility per oxygen added is controlled by dLVP (logarithmic change in vapor pressure) through $\Delta C^* = -\Delta O \times$ dLVP[54]. Lastly, the ageing rate constant of all 2D-VBS products was given by a uniform $k_{OH,Aging}$.

Below we describe the major model developments. Our first update is to account for the first-generation oxidation products explicitly. In the original 2D-VBS model[50], the SOA precursors are mapped directly to some 2D-VBS products based on its C^* and O:C, and its ageing is determined by 2D-VBS parameterizations thereafter. Here we track the precursors separately from the 2D-VBS products and simulate their first-generation oxidation under high-NO_x conditions[46,55] to determine a range of explicit oxidation products informed by GECKO-A[27,56]. Specifically, GECKO-A generates explicit chemical reactions of individual precursors until the formation of first-generation stable products. Because the number of first-generation products can reach hundreds for a given precursor if all the chemical pathways are considered, some reductions are applied, including neglecting chemical pathways with branching ratio lower than 0.5%. For the oxygen-influenced fates of alkoxy radical, we calculate the branching ratios assuming air molecule concentration of 2.5×10^{19} molecules cm^{-3}. Each of the GECKO-A-predicted first-generation products are then mapped into 2D-VBS products based on their predicted C^* and O:C, and multi-generation ageing is taken over by 2D-VBS thereafter. This approach places constraints on the first-generation oxidation chemistry and thus reduces uncertainties in multi-generational ageing.

The second update was to separately simulate the ageing of the 2D-VBS products based on the chemical classes of their precursors. The original model only had one 'layer' of 2D-VBS product matrix, but we expanded the model to include multiple layers of product matrix, each with independent ageing parameters, so that the first-generation products from different primary compounds will enter different layers and age differently, based on the chemical class of their precursors. For wildfire emissions, these classes include heterocyclics, oxygenated aromatics, polycyclic aromatics, benzene-series aromatics, alkanes, terpenes and S/L-VOCs, which are vapours from POA. The ageing parameters of each class were determined separately by fitting to single-species ageing experiments, as discussed in the next section. In summary, the model simulates the multi-generational ageing of all VOC and I/S/L-VOC species by explicitly modelling the first-generation oxidation of all precursors and modelling later-generation oxidation with parameterizations based on the 2D-VBS framework. A text-based representation of all 2D-VBS oxidation reactions have been included as separate supplementary text files.

The updated model also accounts for kinetic gas/particle partitioning, following the diffusive-reactive framework by Zaveri et al.[57], with the bulk diffusivity (D_b) of the particles modulating the rate of gas/particle partitioning. Heterogeneous oxidation is modelled using the kinetic equations from Jathar et al.[58], where the rate of the reaction is governed by the reactive uptake coefficient of the OH at the particle surface (γ_{OH}) and the product distribution for a reacted species is determined identically to gas-phase oxidation. The current model does not explicitly account for the formation of highly oxygenated molecules from the primary compounds through autoxidation, and we do not expect this to substantially impact the model due to the smaller highly oxygenated molecules yield of the wildfire emissions[59]. The model does not account for particle-phase oligomerization reactions due to lack of constraints on rates; the partitioning of particle-phase compound between monomers and oligomers would not substantially impact the modelling of total SOA mass, though O:C may be somewhat lowered by oligomerization[60].

Optimization of ageing parameters for chemical classes

As described in the previous section, there are seven chemical classes for wildfire emissions in the model (eight if including POA), which represent the major classes of precursors in wildfire emissions (Supplementary Table 3). The ageing parameters for each chemical class were determined separately, by fitting to the SOA mass and O:C observed in single-species ageing experiments of representative precursors. The chemical classes and their representative single-species ageing experiments are summarized in Supplementary Table 1. The surrogate species for each class were chosen based on their abundance in wildfire emissions (Supplementary Table 3) and availability of experiment data. For each class, we tried to include experiments from diverse precursors and from both environmental chambers and oxidation flow reactors, when available, to ensure parameter robustness and provide constraints over long-time ageing. For the optimization algorithm, we employed the genetic algorithm[26,61]. We show the fitted predictions for oxygenated aromatics, heterocyclics, benzene-series aromatics, alkanes and polycyclic aromatics in Supplementary Figs. 4 to 8. The fitting for terpenes has been described in a previous work[62].

Modelling SOA formation in the mini-chamber experiments

The mini-chamber experiments were performed as part of the FIREX campaign to investigate the emissions and chemistry of wildfires in the western United States[17,63–65]. The details of the experiments have been described in Lim et al.[17], but a brief overview is given here. The mini chamber was a PFA (perfluoroalkoxy) environmental chamber with a small volume of 150 liters, so it could sustain higher OH levels to reach higher photochemical ages. During each experiment, a biomass fuel was burned, and the emissions were sampled into the mini chamber and comprehensively characterized with a proton-transfer reaction mass spectrometer. Ozone (O_3) injection was then started and continued through the experiment to reach a level of 10–80 ppbv. After well mixing of the emissions, the UV lights were turned on to generate OH from the photolysis of O_3, starting photochemical ageing. The photochemical ageing of the emissions lasted between 30 and 60 min with OH levels on an order of 10^8 molecules cm^{-3}, so the experiments achieved

between 20 and 200 hours of atmospheric ageing (assuming ambient OH of 1.5×10^6 molecules cm^{-3}). The concentration and composition of the OA were monitored online with a scanning mobility particle sizer and aerosol mass spectrometer. Clean air was continuously supplied to the chamber to replace the air removed through instrument sampling, thus resulting in effective dilution of the chamber air. Information on all experiments is given in Supplementary Table 2.

For simulation, we applied the organic emissions profiles based on proton-transfer reaction mass spectrometer measurements for each specific experiment. The unidentified species were neglected, which accounted for a small fraction of all measured organic species (~5%). Supplementary Table 3 summarizes the list of precursors simulated. Initial POA mass concentration was based on Lim et al.[17] and POA volatility distribution was based on May et al.[66], where an amount of S/L-VOCs was assumed to be in equilibrium with POA. The amount of identified S/L-VOC species were subtracted from the assumed S/L-VOC vapours to avoid double counting. The S/L-VOCs aged with the same parameters for oxygenated aromatics, based on measurements of biomass-burning emissions[67,68]. However, sugars and polycyclic aromatics may also be responsible for S/L-VOCs. A sensitivity simulation with S/L-VOCs as polycyclic aromatics (Extended Data Fig. 4) shows a moderate difference in OA and O:C predictions, with reduced SOA contribution from S/L-VOCs. This should represent an extreme scenario, because it is unlikely that all S/L-VOCs are polycyclic aromatics. Future studies need to fully speciate these particle-phase species.

Importantly, we modelled PWL and dilution within the chamber and corrected the model-predicted 'suspended' OA mass for PWL and dilution to facilitate equal comparison with observations. A uniform PWL rate constant ($k_{par,wall} = 4.8 \times 10^{-4}$ s^{-1}) was determined in from a dark experiment where UV was turned off[17]. Dilution was assumed to be a first-order loss and the rate constant was calculated for each experiment based on measured loss of acetonitrile. The dilution rate constants are given in Supplementary Table 2. For model predictions, we let suspended OA be y_1. For dilution, y_1 was divided by a dilution first-order loss curve to find y_2, the dilution-corrected OA mass. The model tracks the OA mass on the wall as y_3. Therefore, the wall loss and dilution-corrected OA mass would be $y_2 + y_3$.

The OH concentrations during the experiments were estimated based on the decay of the dilution-corrected D9-butanol level[69]. The computed OH concentrations started lower at the beginning and reached a peak later in the experiment, due to the continuous addition of O_3. Some experiments showed slight decreases of OH towards the end, which may be an artefact caused by too low a D9-butanol level to be accurately detected. To remove noise, we fitted a curve to the D9-butanol-based estimates (Supplementary Fig. 9) and scaled it to match the reported end-of-experiment OH exposures[17].

The vapour-wall loss rate inside the mini chamber was estimated to be $k_{vap,on} = 5.27 \times 10^{-3}$ s^{-1} or a vapour-wall equilibrium timescale of around 3 minutes. This was based on scaling up from the vapour-wall loss rate of the Colorado State University chamber (10 m^3, $k_{vap,on} = 1.3 \times 10^{-3}$ s^{-1}) (ref. 29), assuming vapour-wall loss rate is proportional to the surface-area-to-volume ratio of the chamber. The vapours were assumed to reversibly partition to the chamber walls[70]. Because the vapour-wall equilibrium timescale is already much shorter than the experiments, uncertainties in the $k_{vap,on}$ value would not substantially influence the modelled SOA. We assume the D_b to be 10^{-10} m^2 s^{-1}, representing a liquid phase state with no limitation on partitioning. This is a reasonable approximation given the moderate relative humidity (30–40% in chamber experiments and higher in the real atmosphere)[71–73]. Heterogeneous oxidation was modelled with γ_{OH} of 0.1, based on measurements for oxygenated particles[74]. The modelled OA was not very sensitive to higher values of γ_{OH} (Extended Data Fig. 5).

Some uncertainties in the mini-chamber experiments may influence SOA formation, which include particle and vapour-wall loss and heterogeneous oxidation. These may vary across experiments due to particle charge (PWL)[17], chamber turbulence (vapour-wall loss)[29,70] and particle-phase state (heterogeneous oxidation)[74], respectively. Because there lacked data to support experiment-by-experiment treatment of these processes, a detailed examination would be for future work. Other uncertainties may include aqueous phase chemistry and photolysis of some organic compounds, which the model does not include. These may not be very important because Lim et al.[17] observed negligible photolysis for some primary SOA precursors, and aqueous chemistry should be a minor pathway for SOA given the moderate relative humidity level (30–40%). Nevertheless, these should be accounted for and examined in future studies.

Modelling SOA formation in real plumes

Supplementary Table 4 summarizes the airborne campaigns that we simulated. The wildfire plumes were intercepted by the aircraft at different distances downwind of the fires in a semi-Lagrangian manner, and therefore the in-plume evolution of OA approximately reflected the influence of photochemical ageing and dilution on a single parcel of emissions. The times of first and last plume transects, counted since emission (Supplementary Table 4), are the points at which the OA excess mixing ratios were calculated to find the OA enhancement ratio. In-plume OH concentrations, typically estimated based on the decay of measured organic species, varied roughly between 5×10^5 and 2×10^7 molecules cm^{-3}. If the OH level was not discussed[47,48], we assumed their average OH level to be equal to the average OH level estimated in Akherati et al.[33] (1.1×10^6 molecules cm^{-3}). Noteworthily, Akherati et al.[33] suggested that the OH level in plumes may be much lower (5–8 times) than previously estimated by including ~120 organic species in their calculation, as opposed to only a few in previous works. Thus, we corrected the OH levels where only a few organic species were used to estimate OH (that is, only eight in Hobbs et al.[46] and one in Akagi et al.[36]) by lowering by a factor of 5. SOA production would be stronger in these two plumes if OH was uncorrected (Supplementary Fig. 10). The time-dependent dilution ratios for most of the plumes were estimated by fitting a one-dimensional dispersion model to the reported CO measurements, following previous studies[35,49]. We also calculated a first-order dilution rate constant (k_{dilu}) for all experiments with CO data, and this first-order loss was applied when the number of CO data points were too few to inform the dispersion model. If CO data were not found[36,39], we assumed a k_{dilu} of 1.5 or 1.15 h^{-1}, which were typical for the studies included here. The OH concentrations and k_{dilu} values for each plume are also summarized in Supplementary Table 4.

We utilized CO-normalized emissions ratios from the 20 FIREX mini-chamber experiments to simulate the SOA formation from these plumes, because complete emissions profiles, especially for I/SVOCs, were not available for these plumes. The emissions ratios were multiplied by an assumed CO of 10 ppmv at the source to find the initial mixing ratios of the organic compounds, based on close-to-fire observations[17,46,48]. Though, because POA and SOA precursor both scale with the CO emissions, the ΔOA/ΔCO enhancement in plume should be relatively free of the assumed CO value, which typically vary between 4 and 15 ppmv. Overall, for each plume and each scenario, 20 simulations were performed with different FIREX-based emissions ratios, and the ΔOA/ΔCO predictions were averaged across these simulations. The variability in these emissions profiles was assumed to reflect the uncertainties in ΔOA/ΔCO enhancement with respect to emissions because the mini-chamber experiments covered diverse types of fuel (Supplementary Table 2), with modified combustion efficiency varying between 0.78 and 0.96, indicating smouldering to flaming.

Estimation of long-time SOA evolution and global SOA production

We estimated long-time SOA evolution and global SOA production through Monte Carlo simulations (500 repetitions). To do this, we estimated the global distributions of organic emissions profiles and

dilution rates. Most field measurements of wildfire emissions profiles lacked characterization of the I/SVOCs. The emissions profiles from the FIREX campaign were one of the only ones that comprehensively measured I/SVOCs. Thus, we applied the mean of the FIREX emissions profiles but needed to know how it possibly compared to the global mean and standard deviations. We estimated the global mean of wildfire emissions of some volatile organic compounds based on biome-specific emissions profiles (savannah/grassland, temperate forest, boreal forest, tropical forest and peat)[24,75], weighted by the total carbon emissions[75] from each biome. As shown in Extended Data Fig. 6a, the FIREX-average profile correlated well with the estimated global-average profile, and the mean values were close. The standard deviation of the FIREX-average profile did not fully cover the standard deviation of the global-average profile; thus, we magnified the standard deviation of the FIREX profile by 1.5 to roughly cover the uncertainty in the global-average profile. We also show the emissions profiles from different biomes in Extended Data Fig. 6b. There is some emission variability between different biomes, but the magnitude of the difference is mostly less than the level of uncertainty within each biome, which may be caused by different burning conditions and other environmental factors[24]. Thus, the impact of specific biome type on wildfire SOA formation is still uncertain without fixing the other factors, and the use of the FIREX-average emissions profile with enlarged standard deviation to capture the global emissions profile should suffice current estimations. In Supplementary Fig. 3, we show estimated ΔOA/ΔCO enhancement ratios from each biome type by applying the emissions ratios of VOC and I/SVOC precursors of SOA from Andreae[24] to the FIREX-average emissions profile. The biome-specific enhancement ratios are only moderately different from the average of the Monte Carlo simulations and well within the uncertainty range. The dilution rate was estimated with an eddy dispersion model[35,49], and it mainly varies with the size of the fire. Here we assumed the global fire-size distribution of area burned followed the US fire distribution from Hodshire et al.[1]. A dilution rate profile was calculated for each fire size, assuming an eddy diffusivity of 7,000 $m^2 s^{-1}$(refs. 35,49) (Supplementary Fig. 11); it is shown that large fires dilute more slowly than small fires. Each simulation was run up to 200 equivalent hours of photochemical ageing. The OH concentration was prescribed with that estimated in Akherati et al.[33] (Supplementary Fig. 12), but to account for potential uncertainties, we multiplied the OH level with a scaling factor sampled from 1/3 to 3 with equal probability. Note that because we show SOA evolution in terms of equivalent photochemical age, the absolute OH level should not change ΔOA/ΔCO curve in Fig. 4a, albeit modifying the relative importance of dilution.

Data availability

All data displayed in the figures are archived at https://figshare.com/projects/wildfire2023/178356.

Code Availability

Codes for the precursor-resolved 2D-VBS-MOSAIC model can be obtained from the corresponding author upon request.

References

50. Chuang, W. K. & Donahue, N. M. A two-dimensional volatility basis set—part 3: prognostic modeling and NO_x dependence. *Atmos. Chem. Phys.* **16**, 123–134 (2016).
51. Zhao, B. et al. Quantifying the effect of organic aerosol aging and intermediate-volatility emissions on regional-scale aerosol pollution in China. *Sci. Rep.* **6**, 28815 (2016).
52. Schervish, M. & Donahue, N. M. Peroxy radical chemistry and the volatility basis set. *Atmos. Chem. Phys.* **20**, 1183–1199 (2020).
53. Zaveri, R. A., Easter, R. C., Fast, J. D. & Peters, L. K. Model for simulating aerosol interactions and chemistry (MOSAIC). *J. Geophys. Res.* **113**, D13204 (2008).
54. Cappa, C. D. & Wilson, K. R. Multi-generation gas-phase oxidation, equilibrium partitioning, and the formation and evolution of secondary organic aerosol. *Atmos. Chem. Phys.* **12**, 9505–9528 (2012).
55. Alvarado, M. J., Wang, C. & Prinn, R. G. Formation of ozone and growth of aerosols in young smoke plumes from biomass burning: 2. three-dimensional Eulerian studies. *J. Geophys. Res.* **114**, D09307 (2009).
56. Lannuque, V., Couvidat, F., Camredon, M., Aumont, B. & Bessagnet, B. Modeling organic aerosol over Europe in summer conditions with the VBS-GECKO parameterization: sensitivity to secondary organic compound properties and IVOC (intermediate-volatility organic compound) emissions. *Atmos. Chem. Phys.* **20**, 4905–4931 (2020).
57. Zaveri, R. A., Easter, R. C., Shilling, J. E. & Seinfeld, J. H. Modeling kinetic partitioning of secondary organic aerosol and size distribution dynamics: representing effects of volatility, phase state, and particle-phase reaction. *Atmos. Chem. Phys.* **14**, 5153–5181 (2014).
58. Jathar, S. H. et al. A computationally efficient model to represent the chemistry, thermodynamics, and microphysics of secondary organic aerosols (simpleSOM): model development and application to α-pinene SOA. *Environ. Sci. Atmos* **1**, 372–394 (2021).
59. Bianchi, F. et al. Highly oxygenated organic molecules (HOM) from gas-phase autoxidation involving peroxy radicals: a key contributor to atmospheric aerosol. *Chem. Rev.* **119**, 3472–3509 (2019).
60. He, Y. et al. Particle size distribution dynamics can help constrain the phase state of secondary organic aerosol. *Environ. Sci. Technol.* **55**, 1466–1476 (2021).
61. Gad, A. F. PyGAD: an intuitive genetic algorithm Python library. Preprint at http://arxiv.org/abs/2106.06158 (2021).
62. Zhao, B. et al. Evaluation of one-dimensional and two-dimensional volatility basis sets in simulating the aging of secondary organic aerosol with smog-chamber experiments. *Environ. Sci. Technol.* **49**, 2245–2254 (2015).
63. Koss, A. R. et al. Non-methane organic gas emissions from biomass burning: identification, quantification, and emission factors from PTR-ToF during the FIREX 2016 laboratory experiment. *Atmos. Chem. Phys.* **18**, 3299–3319 (2018).
64. Hatch, L. E. et al. Identification and quantification of gaseous organic compounds emitted from biomass burning using two-dimensional gas chromatography–time-of-flight mass spectrometry. *Atmos. Chem. Phys.* **15**, 1865–1899 (2015).
65. Sekimoto, K. et al. High- and low-temperature pyrolysis profiles describe volatile organic compound emissions from western US wildfire fuels. *Atmos. Chem. Phys.* **18**, 9263–9281 (2018).
66. May, A. A. et al. Gas-particle partitioning of primary organic aerosol emissions: 3. biomass burning. *J. Geophys. Res. Atmos.* **118**, 11,327–11,338 (2013).
67. Jen, C. N. et al. Speciated and total emission factors of particulate organics from burning western US wildland fuels and their dependence on combustion efficiency. *Atmos. Chem. Phys.* **19**, 1013–1026 (2019).
68. Huang, G. et al. Emission factors and chemical profile of I/SVOCs emitted from household biomass stove in China. *Sci. Total Environ.* **842**, 156940 (2022).
69. Barmet, P. et al. OH clock determination by proton transfer reaction mass spectrometry at an environmental chamber. *Atmos. Meas. Tech.* **5**, 647–656 (2012).
70. Krechmer, J. E., Pagonis, D., Ziemann, P. J. & Jimenez, J. L. Quantification of gas-wall Partitioning in Teflon environmental chambers using rapid bursts of low-volatility oxidized species generated in situ. *Environ. Sci. Technol.* **50**, 5757–5765 (2016).

71. Shiraiwa, M. et al. Global distribution of particle phase state in atmospheric secondary organic aerosols. *Nat. Commun.* **8**, 15002 (2017).
72. Li, Y., Day, D. A., Stark, H., Jimenez, J. L. & Shiraiwa, M. Predictions of the glass transition temperature and viscosity of organic aerosols from volatility distributions. *Atmos. Chem. Phys.* **20**, 8103–8122 (2020).
73. Kiland, K. J. et al. Viscosity, glass formation, and mixing times within secondary organic aerosol from biomass burning phenolics. *ACS Earth Space Chem*. https://doi.org/10.1021/acsearthspacechem.3c00039 (2023).
74. Li, J. & Knopf, D. A. Representation of multiphase OH oxidation of amorphous organic aerosol for tropospheric conditions. *Environ. Sci. Technol*. **55**, 7266–7275 (2021).
75. Van Der Werf, G. R. et al. Global fire emissions estimates during 1997–2016. *Earth Syst. Sci. Data* **9**, 697–720 (2017).

Acknowledgements

We thank J. H. Kroll and C. Y. Lim for providing the mini-chamber experiment data and for helpful data-related discussions. This work is supported by National Natural Science Foundation of China (22188102; B.Z. and S.W.) and Samsung Advanced Institute of Technology (Y.H., X.C., D.Y., B.Z. and S.W.). C.D.C. was supported by the California Air Resources Board (contract 18RD009). M.S. was supported by the US Department of Energy (DOE) Office of Science, Office of Biological and Environmental Research (BER) through the Early Career Research Program and DOE BER's Atmospheric System Research programme. The Pacific Northwest National Laboratory is operated for DOE by Battelle Memorial Institute under contract DE-AC06-76RL01830. S.H.J. was supported by Assistance Agreement number R840008 awarded by the US Environmental Protection Agency to Colorado State University. This work has not been formally reviewed by EPA. The views expressed in this document are solely those of the authors and do not necessarily reflect those of the Agency. EPA does not endorse any products or commercial services mentioned in this publication.

Author contributions

Y.H., B.Z., S.W. and J.H. designed the study. Y.H. and B.Z. led model development. D.Y., X.C., R.V., M.C. and B.A. contributed to model development. B.F., A.D., S.H.J., L.D.Y. and J.H.S. provided experimental data. A.D. and S.H.J. helped with experimental data analysis. Y.H., B.Z. and S.W. wrote the paper with contributions from M.S., Z.J., C.D.C., N.M.D. and all other co-authors.

Competing interests

The authors declare no competing interests.

Additional information

Extended data is available for this paper at https://doi.org/10.1038/s41561-023-01355-4.

Supplementary information The online version contains supplementary material available at https://doi.org/10.1038/s41561-023-01355-4.

Correspondence and requests for materials should be addressed to Bin Zhao.

Peer review information *Nature Geoscience* thanks Marwa Majdi and the other, anonymous, reviewer(s) for their contribution to the peer review of this work. Primary Handling Editor: Xujia Jiang, in collaboration with the *Nature Geoscience* team.

https://doi.org/10.1038/s41561-023-01355-4

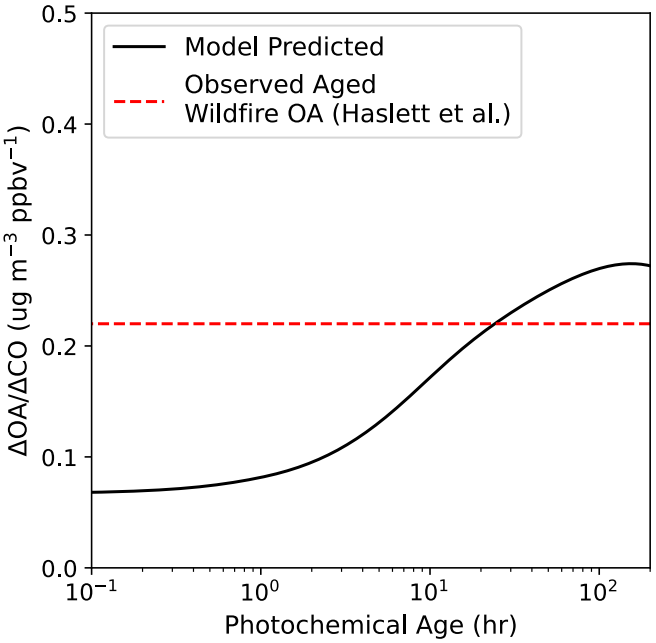

Extended Data Fig. 1 | Model Comparison with Observed Highly Aged Wildfire OA in West Africa. The model-predicted ΔOA/ΔCO is the average of the 500 Monte Carlo simulations and is compared to measurements inside highly aged biomass-burning aerosol layer in the free troposphere above western Africa[38].

https://doi.org/10.1038/s41561-023-01355-4

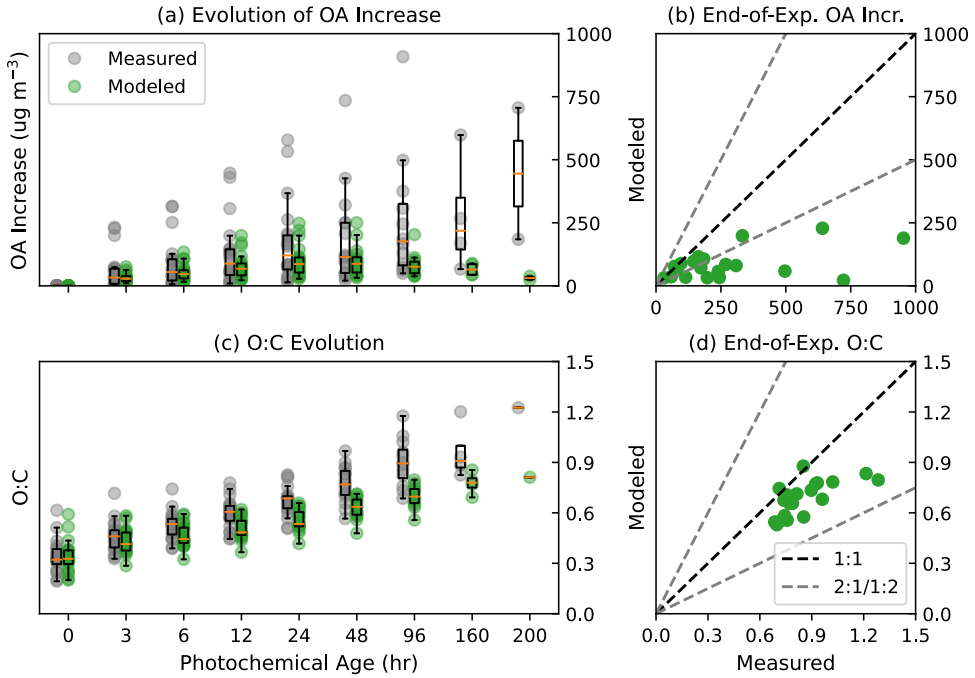

Extended Data Fig. 2 | Same as Fig. 1 but with all I/SVOCs Lumped as Alkanes. In comparison to simulating the specific I/SVOC precursors and their chemical classes, the increase in OA is greatly under-predicted and the O:C prediction are also affected. The box plots in (a) and (c) show distributions of each group of data points, including 20 experiments, at the 5% (lower whisker), 25% (box lower bound), 50% (box center line), 75% (box upper bound) and 95% (upper whisker) percentiles. The photochemical age is the integrated OH exposure divided by a typical atmospheric OH level (1.5×10^6 molecules cm^{-3}). (b) and (d) show the model-measurement comparison at the end of experiments.

https://doi.org/10.1038/s41561-023-01355-4

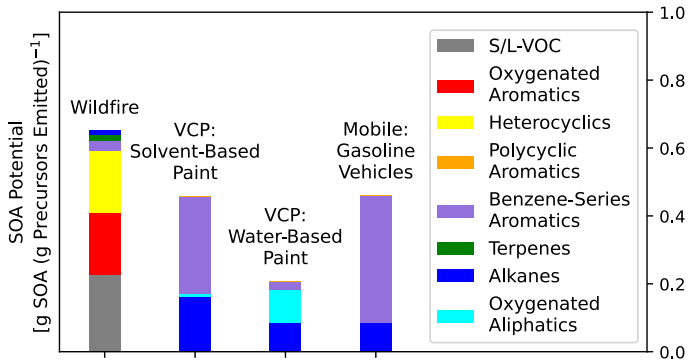

Extended Data Fig. 3 | Predicted SOA Forming Potentials of Different Emission Sources by the Precursor-Resolved 2D-VBS-MOSAIC Model. Initial emission from each source was aged for 48 hours and gas/particle partitioning was evaluated at a background OA of 10 μg m^{-3}. The emission profiles for the VCP and mobile sources were based on experimental measurements.

https://doi.org/10.1038/s41561-023-01355-4

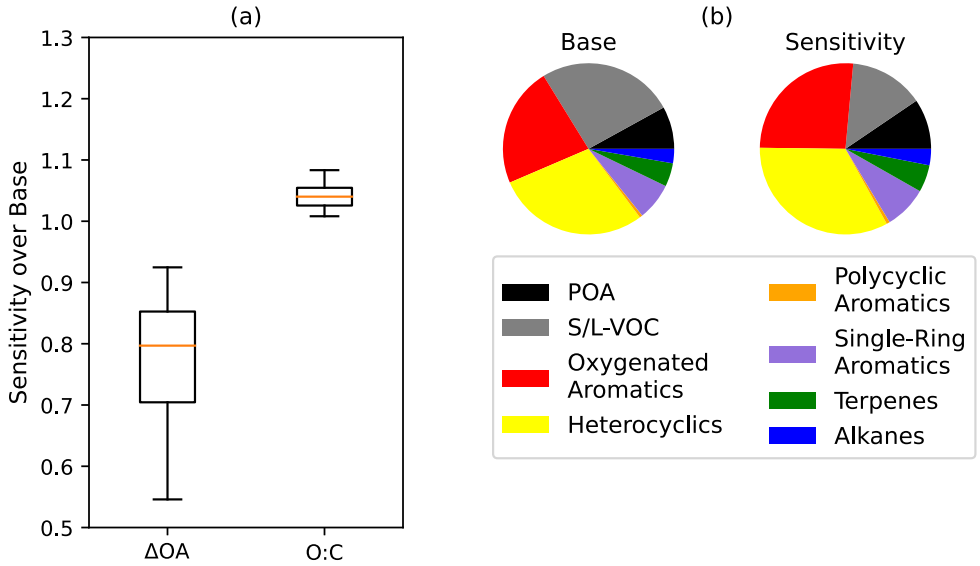

Extended Data Fig. 4 | Model Sensitivity to I/SVOC Treatment. (**a**) shows the ratio between ΔOA and O:C prediction from the sensitivity case and the base case for the mini-chamber experiments. The base case treats S/L-VOCs as oxygenated aromatics and the sensitivity case treats them as polycyclic aromatics. (**b**) shows the averaged precursor contributions at the end of the experiments. The box plots in (a) include 20 experiments and show the 5% (lower whisker), 25% (box lower bound), 50% (box center line), 75% (box upper bound) and 95% (upper whisker) percentiles.

https://doi.org/10.1038/s41561-023-01355-4

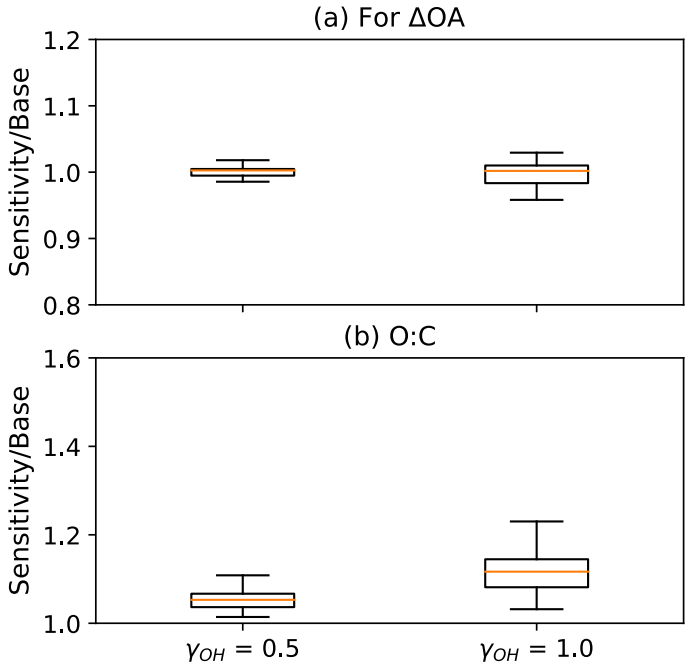

Extended Data Fig. 5 | Model sensitivity to Heterogeneous Oxidation. The base case (that is, as shown in Fig. 1) assumed $\gamma_{OH} = 0.1$. The box plots in (**a**) and (**b**) include 20 experiments and show the 5% (lower whisker), 25% (box lower bound), 50% (box center line), 75% (box upper bound) and 95% (upper whisker) percentiles.

https://doi.org/10.1038/s41561-023-01355-4

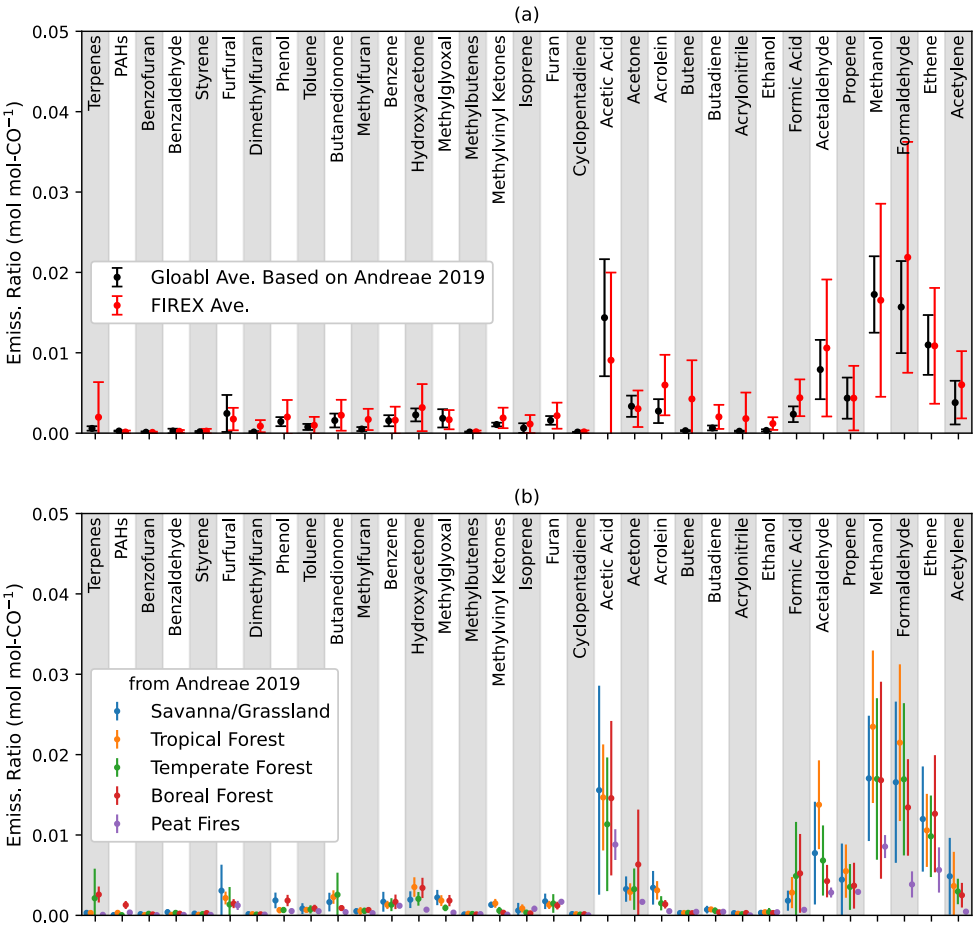

Extended Data Fig. 6 | FIREX and Global Emission Profiles. (**a**) comparison between the averaged emission profiles from the 20 FIREX experiments and the estimated global-average profile based on Andreae6 for the species that exist in both profiles. The FIREX emission profile contains 20 data points for each species and the emission ratios are shown in mean value +/− 1.5 times standard deviation. The standard deviations of the FIREX profile have been multiplied by 1.5 to encompass the uncertainty range of the estimated global-average profile. For the Andreae profile[6], the emission ratios are shown in mean value +/− one standard deviation and the number of data points varies by species; see the reference for more details. (**b**) the emission profiles of the different types of biomes from Andreae[6], showing only the species that also exist in the FIREX profile.